J Mater Sci (2008) 43:6872–6880
DOI 10.1007/s10853-008-3011-5

The Fe–Zn–Al–Cr system and its impact on the galvanizing process in chromium-added zinc baths

Richard Fourmentin · Marie-Noëlle Avettand-Fènoël · Guy Reumont · Pierre Perrot

Received: 10 July 2008 / Accepted: 17 September 2008 / Published online: 11 October 2008

Abstract The zinc rich corner of the Fe–Zn–Al–Cr at 460 °C is of interest for galvanizing because Al is a usual addition element in zinc bath, whereas Cr is naturally present because it is supplied by the stainless steel roller dipping in the Zn bath during the process. Indeed, it is used to understand the formation and growth mechanisms of the solid phases during galvanizing in Al and Cr-added Zn bath. By using additional experimental results in the Al–Cr–Zn and Fe–Zn–Al–Cr systems, the zinc rich corner of the Fe–Zn–Al–Cr system at 460 °C was determined with more accuracy. Thus, new equilibria between the liquid and quaternary phases have been pointed out, namely Al_2Cr_3 stabilized by Zn and enriched with Fe and τ_1, the latter being isotypic with δ-$FeZn_9$. This quaternary system was assessed with the CALPHAD method using the PARROT module of the Thermo-Calc Software. The liquid and solid solutions are described by the Redlich-Kister-Muggianu equations. All the modeled phases are considered as stoichiometric in the binary systems.

Introduction

Aluminum has been added to the zinc bath to prevent over thickness of the galvanizing coatings. Chromium is not an element normally added to the bath but is often present from immerged equipment. The steel strips used in automotive industry are currently continuously galvanized at 460 °C. The presence of Al in the zinc bath, between 0.135 and 0.200 mass%, improves the mechanical characteristics of the coating by delaying the nucleation of brittle Fe–Zn compounds with the formation of an inhibition layer. The latter is composed of the Fe_2Al_5 intermetallic compound containing about 15 mass% Zn [1]. The control of equilibrium between the liquid phase (zinc bath) and the solid phases (both galvanized coating and precipitates in the bath) is possible by using the Fe–Zn–Al–Cr phase diagram at 460 °C. However, the development of this quaternary diagram first requires the study of the three other ternary diagrams in the zinc rich corner. Fe–Zn–Al diagram which is experimentally well-known [2–6] has been thoroughly assessed by different authors [7–9]. Fe–Cr–Zn system was experimentally investigated in the Zn rich corner [10, 11] and recently reviewed by Raghavan [12]. According to us, the Al–Cr–Zn phase diagram was only reported in two studies [13, 14]. These diagrams were experimentally investigated then calculated using the Calphad method. The main advantage of a modeled phase diagram is to obtain a reliable assessment of the liquid/solids equilibria at 460 °C irrespective of industrial parameters (temperature and composition of the bath). The zinc rich corners of the systems Al–Cr–Zn, Fe–Zn–Cr and Fe–Zn–Al have been modeled elsewhere [13, 15, 16]. The optimization of the quaternary system has been carried out using the description obtained from the ternary systems. In addition, no quaternary parameter has been added because the experimental solubilities agree with the calculated ones and the iron, chromium, and aluminum contents are very low in the zinc bath.

R. Fourmentin · M.-N. Avettand-Fènoël · G. Reumont · P. Perrot (✉)
Laboratoire de Metallurgie Physique et Genie des Materiaux, UMR CNRS 8517, Université de Lille I, 59655 Villeneuve d'Ascq Cedex, France
e-mail: pierre.perrot@univ-lille1.fr

Experimental results

The optimization of the Fe–Zn–Al–Cr isothermal liquidus surface at 460 °C required a preliminary experimental study of this quaternary system. First, iron and chromium plates were galvanized in Al–Cr–Zn baths saturated with iron at 460 °C, then chromium or iron was gradually added in baths at 460 °C. In these experiments, the compositions of these baths are consistent with aluminum contents commonly used in industrial processes (i.e., $0.135 < \text{mass\% Al} < 0.200$). Chromium contents (Table 1) were fixed in order to obtain numerous equilibria between phases. The liquid phase of the baths was separated by filtration from the intermetallic solid impurities called floating or bottom dross according to their density then analyzed by Inductively Coupled Plasma (ICP). The solid phases and dross were observed by Scanning Electron Microscope (SEM) and analyzed by Energy Dispersive Spectroscopy (EDS). Dross were also extracted from their solidified zinc matrix by zinc evaporation [17] to be studied by X-Ray Diffractometry (XRD).

Table 1 Compositions of the baths used for galvanization

Bath	A	B	C	D	E	F	G	H	I
mass% Al	0.25	0.20	0.13	0.13	0.20	0.20	0.20	0.20	0.25
mass% Cr	0.25	0.30	0.07	0.20	0.03	0.07	0.20	0.25	0.30

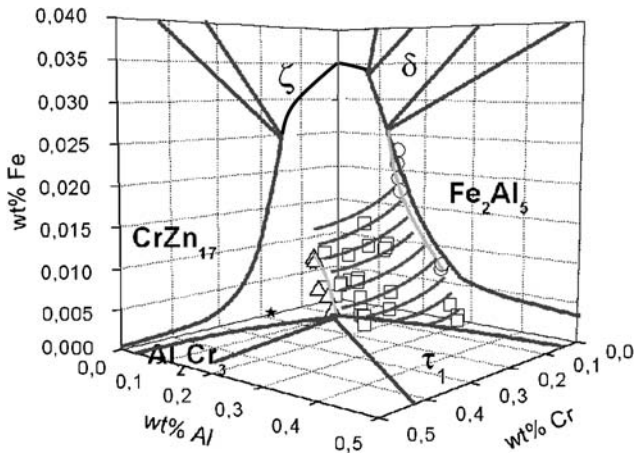

Fig. 1 Liquidus of the Fe–Zn–Al–Cr system at 460 °C. The meaning of the symbol is given in the text

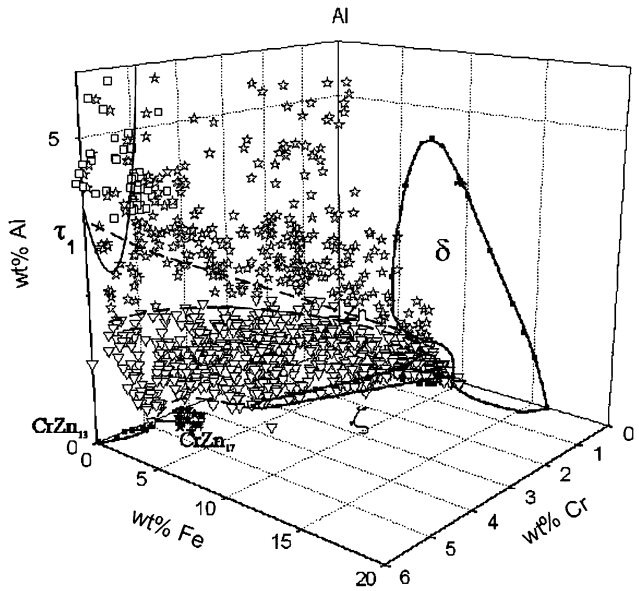

Fig. 2 Zinc-rich corner of the Fe–Zn–Al–Cr system at 460 °C. The meaning of the symbol is given in the text

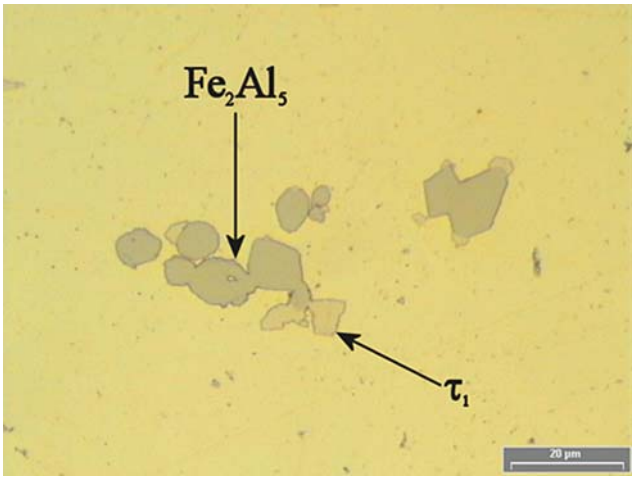

Fig. 3 $Fe_2(Al_{1-x}Zn_x)_5$ and $\delta(\tau_1)$ compounds precipitation in the 0.30 mass% Al–0.05 mass% Cr bath

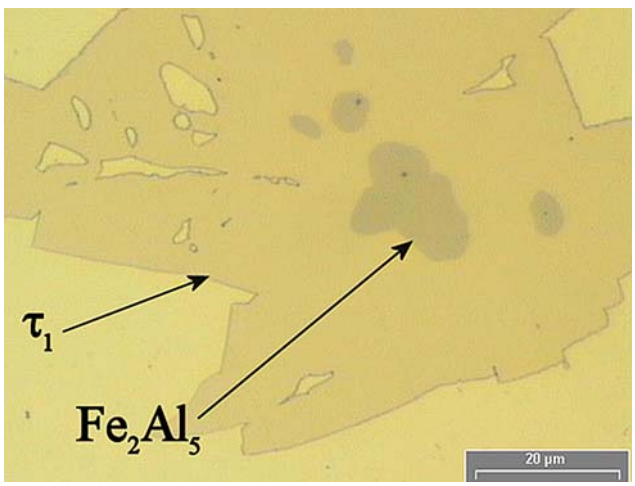

Fig. 4 $Fe_2(Al_{1-x}Zn_x)_5$ and $\delta(\tau_1)$ compounds precipitation in the 0.30 mass% Al–0.10 mass% Cr bath

Table 2 Solid phases stable at 460 °C

Phase Stability range (°C)	Pearson symbol Space group Prototype	Crystal parameters (pm)	Remarks
(Al) <660.452	*cF*4 *Fm*-3*m* Cu	$a = 404.96$	Pure Al at 20 °C. Dissolves 43 at% Zn at 460 °C [20]
(αFe) <1,538	*cI*2 *Im*-3*m* W	$a = 286.65$	Pure Fe at 20 °C. Dissolves 7 at% Cr, 5 at% Zn and 49 at% Al at 460 °C [20]
(Cr) <1,983		$a = 288.48$	Pure Cr at 20 °C. Dissolves 11 at% Fe and 5 at% Al at 460 °C [20]
(Zn) <419.58	*hP*2 $P6_3/mmc$ Mg	$a = 266.50$ $c = 494.70$	Liquid Zn dissolves 33 at% Al, 1.1 t% Cr, and 0.035 at% Fe at 460 °C [20]
Γ_1 <782	*cI*52 *I*-43*m* Cu_5Zn_8	$a = 898.2$	72–77 at% Zn at 460 °C [21]
Γ_2 <550	*cF*408 *F*-43*m* Fe_3Zn_{10}	$a = 1{,}796.3$	81–83 at% Zn at 460 °C [21], ordered Cu_5Zn_8 structure
δ <665	*hP*555 $P6_3/mc$	$a = 1{,}277.4$ $c = 5{,}696.7$ $a = 1{,}280.1$ $c = 5{,}730.3$	88–92.5 at% Zn at 460 °C At 88 at% Zn [21] At 92 at% Zn
τ_1,$Cr(Al_xZn_{1-x})_9$			$0.1 < x < 0.33$
		$a = 1{,}282.2$ $c = 5{,}051.0$	$x = 0.33$ (present work)
ζ,$FeZn_{13}$ <530	*mC*28 *C*2/*m* $CoZn_{13}$	$a = 1{,}342.4$ $b = 760.8$ $c = 506.1$ $\beta = 127.3°$	93 at% Zn at 460 °C [21]
ζ,$(Fe_{1-x}Cr_x)Zn_{13}$			$0 < x < 0.1$ and $0.2 < x < 1$
ζ,$CrZn_{13}$			93 at% Zn at 460 °C [22]
$CrZn_{17}$ <464	*hP**	$a = 1{,}291.6$ $c = 3{,}056.2$	[22]
$Cr(Zn_{1-x}Fe_x)_{17}$			$x < 0.1$
Al_7Cr <795	*mC*104 *C*2/*m* $Al_{45}V_7$	$a = 2{,}519.6$ $b = 757.4$ $c = 1{,}094.9$ $\beta = 128.7°$	12.4–13.7 at% Cr [23] Sometimes labeled $Al_{13}Cr_2$
Al_5Cr <865	*mC**	$a = 1{,}760$ $b = 3{,}050$ $c = 1{,}760$ $\beta = 90$	15.2–17 at% Cr [23] Pseudo quadratic phase, sometimes labeled $Al_{11}Cr_2$

Table 2 continued

Phase Stability range (°C)	Pearson symbol Space group Prototype	Crystal parameters (pm)	Remarks
Al_4Cr <1,040	*hP** *P6*$_3$*/mmc* Al_4Cr	$a = 2{,}000$ $c = 2{,}470$	18.7–21.3 at% Cr [23]
Al_9Cr_4	*cI*52 *I*-43*m* Al_9Cr_4	$a = 912.3$	30–33.5 at% Cr At 30.9 at% Cr [24]
Al_8Cr_5	*hR*26 *R*-3*m* Al_8Cr_5	$a = 1{,}275$ $c = 795$	[25], γ-brass (Cu_5Zn_8) rhomboedrically distorded
Al_2Cr_3 $Al_2(Cr_{1-x}Zn_x)_3$			60 at% Cr, metastable. Stabilized by Zn [13] $0.01 < x < 0.15$
$AlCr_2$	*tI*6 *I*4/*mmm* $MoSi_2$	$a = 300.45$ $c = 864.77$	65.5–71 at% Cr [24]
$FeAl_2$ <1,160	*aP*18 *P*1 $FeAl_2$	$a = 760.9$ $b = 1{,}691.6$ $c = 486.9$	$\alpha = 89.49°$, $\beta = 122.65°$, $\gamma = 90.54°$, JCPDS file 33-0019
Fe_2Al_5 <1,169 $Fe_2(Al_{1-x}Zn_x)_5$	*oC*56 *Cmcm* Fe_2Al_5	$a = 767.5$ $b = 640.3$ $c = 420.3$	[21, 24] $x < 0.15$
$FeAl_3$ <1,160	*mC*102 *C*2/*m*	$a = 1{,}548.9$ $b = 808.3$ $c = 1{,}247.6$ $\beta = 107.72°$	[21, 24]

The liquidus description of the quaternary system Fe–Zn–Al–Cr at 460 °C was deduced from that of ternary systems Fe–Zn–Al, Fe–Zn–Cr and Al–Cr–Zn at 460 °C by taking into account the ICP measurements. Two monovariant three-phase equilibria were observed, namely liquid + Al_2Cr_3 + τ_1 and liquid + Fe_2Al_5 + τ_1 (symbolized by Δ and $\bigcirc$ respectively, in Fig. 1) and one two-phase equilibrium liquid + τ_1 (symbolized by $\square$ in Fig. 1). According to analyses, liquid phase may be in equilibrium with 6 intermetallic compounds namely δ-$FeZn_9$, ζ-$FeZn_{13}$, $CrZn_{17}$, Al_2Cr_3, Fe_2Al_5, and τ_1. δ and ζ belong to the Fe–Zn binary and may be enriched with Al and Cr. The Fe_2Al_5 compound is actually saturated with zinc. $CrZn_{17}$ may dissolve a small amount of iron which substitutes zinc in the lattice. Finally, τ_1 is a ternary phase of the Al–Cr–Zn system, whose crystal structure is isotypic with δ (Fig. 1). The solid phase Al_2Cr_3 presents the particularity of being a metastable phase of the Al–Cr binary which is stabilized by zinc [13]. The chromium solubility in Fe_2Al_5 has been measured at 0.4 mass%. It must be pointed out that the phase $FeAl_3$ may be in equilibrium with an Al rich liquid zinc bath. Actually, galvanizing baths containing less than 1 mass% Al, cannot be in equilibrium with $FeAl_3$.

From EDS analyses of solid phases, the zinc rich corner of the Fe–Zn–Al–Cr system at 460 °C is presented in Fig. 2. This 3-D visualization allowed us to identify the monophased domains in the quaternary Fe–Zn–Al–Cr system. The stability domain of the intermetallic compound ζ (∇) is continuous from ζ-$FeZn_{13}$ to $CrZn_{13}$ where Cr atoms substitute Fe atoms in the monoclinic structure. The ζ domain is only split by the small stability domain of the $(Cr,Fe)Zn_{17}$ phase (★) in the Fe–Cr–Zn plane. Indeed, the Al solubility in $(Cr,Fe)Zn_{17}$ is too low to be measured by EDS. Figure 2 presents also a cloud of experimental points (☆) linking

Table 3 Assessed thermodynamical parameters of the liquid and solid solutions

Solution	Description	Interaction parameter	Value	References
Liquid	(Al,Cr,Fe,Zn)	Fe–Cr	$L_0 = -14{,}550 + 6.65*T$	
		Fe–Zn	$L_0 = 61{,}769.4919 - 27.2621615*T$	[10]
			$L_1 = 70{,}131.5078 - 42.0466672*T$	
		Al–Fe	$L_0 = -91{,}976.5 + 22.1314*T$	[16]
			$L_1 = -5{,}672.58 + 4.8728*T$	
			$L_2 = 121.9$	
		Cr–Zn	$L_0 = 4{,}528$	[15]
			$L_1 = -1{,}000$	
		Al–Cr	$L_0 = -9{,}552 - 30*T$	[26]
			$L_1 = 2{,}946 - 14*T$	
			$L_2 = -12{,}000$	
		Al–Zn	$L_0 = 10{,}288 - 3.035*T$	[16]
			$L_1 = -810 + 0.471*T$	
BCC-A2	$(Al,Cr,Fe,Zn)_1(Va)_3$	Cr–Fe	$L_0 = 20{,}500 - 9.68*T$	[10]
		Fe–Zn	$L_0 = 7.40254406*T$	[10]
			$L_1 = 2{,}688.41702 - 0.286554146*T$	
		Cr–Zn	$L_0 = 80*T$	[15]
		Al–Cr	$L_0 = -55{,}370 - 10*T$	[26]
			$L_1 = 1{,}830–10*T$	
			$L_2 = -8{,}800$	
FCC-A1	$(Al,Cr,Fe,Zn)_1(Va)_1$	Cr–Fe	$L_0 = 10{,}833 - 7.477*T$	[10]
			$L_1 = 1{,}410$	
		Al–Fe	$L_0 = -76{,}066.1 + 18.6758*T$	[16]
			$L_1 = 21{,}167.4 + 1.3398*T$	
		Fe–Zn	$L_0 = 10{,}861.8262 - 1.5187374*T$	[10]
		Al–Cr	$L_0 = -63{,}800 - 5*T$	[26]
			$L_1 = 8{,}000$	
			$L_2 = -4{,}000$	
		Al–Zn	$L_0 = -7{,}297.48 + 0.47512*T$	[16]
			$L_1 = 6{,}612.88 - 4.5911*T$	
			$L_2 = -3{,}097.19 + 3.30635*T$	
		Cr–Zn	$L_0 = 0$	[15]
HCP-A3	$(Al,Cr,Fe,Zn)_1(Va)_{0.5}$	Fe–Zn	$L_0 = 17{,}635.422$	[10]
		Cr–Fe	$L_0 = 10{,}833 - 7.477*T$	[10]
		Al–Zn	$L_0 = 18{,}820.95 - 8.95255*T$	[16]
		Cr–Zn	$L_0 = 80*T$	[15]

continuously the δ and τ_1 ($\square$) domains. The δ phase in the Fe–Zn–Al system is well known; the τ_1 phase in the Al–Zn–Cr system was previously described in [13]. As a consequence, δ and τ_1 form a continuous solid solution. This identification $\delta = \tau_1$ was confirmed by the XRD pattern of both phases, which crystallize in the hexagonal $P6_3/mc$ system. In the further studies, the solid solutions δ–τ_1 will be labeled δ.

The SEM observations of the solid phases obtained by gradual addition of iron give useful information about the growth process of the solid phases. Given the Al content (0.30 mass%), for low chromium content (0.05 mass% Cr), the iron addition precipitates Fe_2Al_5 and δ (Fig. 3) whereas for high chromium content (0.10 mass% Cr), the precipitation of Fe_2Al_5 is observed inside δ as shown in Fig. 4.

Thermodynamical assessment

Optimizations and calculations have been carried out under 0.1 MPa using Thermo-Calc software [18]. The optimized

Table 4 Assessed thermodynamical parameters of the intermetallic compounds

Intermetallic compound	Description	Interaction parameter (IP) or not	Value	References
ζ	$(Al,Cr,Fe)_{0.072}(Al,Zn)_{0.928}$	Fe–Zn	$\Delta G^{f}_{Fe-Zn} = -3,035$	[10]
		Fe–Al	$\Delta G^{f}_{Fe-Al} = -4,300$	This work
		Al–Zn	$\Delta G^{f}_{Al-Zn} = -1,250$	[16]
		Cr–Zn	$\Delta G^{f}_{Cr-Zn} = -595 - 0.282 \times T$	[15]
		Cr,Fe:Zn (IP)	$L_0 = -1{,}206.57397$	[10]
		Al,Cr:Zn (IP)	$L_0 = -1{,}000$	[13]
$\delta(\tau_1)$	$(Al,Cr,Fe)_{0.125}(Al,Zn)_{0.295}(Zn)_{0.58}$	Fe–Zn	$\Delta G^{f}_{Fe-Zn} = -4352.6 + 0.6074 \times T$	[10]
		Cr–Zn	$\Delta G^{f}_{Cr-Zn} = -400$	[15]
		Al–Cr–Zn	$\Delta G^{f}_{Al-Cr-Zn} = -9,000$	[13]
		Cr,Fe:Zn (IP)	$L_0 = -1{,}206.57397$	[10]
		Al,Zn:Fe:Zn (IP)	$L_0 = -5{,}5380$	This work
Γ_1	$(Fe)_{0.25}(Zn)_{0.75}$	Fe–Zn	$\Delta G^{f}_{Fe-Zn} = -8,497.68457 + 3.876259 \times T$	[10]
Γ_2	$(Fe)_{0.2}(Zn)_{0.8}$	Fe–Zn	$\Delta G^{f}_{Fe-Zn} = -7,324.97391 + 3.02901415 \times T$	[10]
$CrZn_{17}$	$(Al,Cr)_{0.0556}(Fe,Zn)_{0.9444}$	Cr–Fe	$\Delta G^{f}_{Cr-Fe} = 4,500$	[15]
		Cr–Zn	$\Delta G^{f}_{Cr-Zn} = -565 - 0.382 \times T$	[15]
		Al–Zn	$\Delta G^{f}_{Al-Zn} = -300$	[16]
		Al,Cr:Zn (IP)	$L_0 = -1{,}500$	[13]
		Cr:Fe,Zn (IP)	$L_0 = 974{,}132.663$	This work
			$L_1 = 1{,}062{,}315.63$	
Al_5Fe_2	$(Al,Zn)_{0.714}(Fe)_{0.286}$	Fe–Al	$\Delta G^{f}_{Fe-Al} = -33253.7 + 6.99929 \times T$	[16]
		Fe–Zn	$\Delta G^{f}_{Fe-Zn} = -2,050$	[16]
Al_2Fe	$(Al,Zn)_{0.663}(Fe)_{0.337}$	Fe–Al	$\Delta G^{f}_{Fe-Al} = -32,836.3 + 6.2501 \times T$	[16]
		Fe–Zn	$\Delta G^{f}_{Fe-Zn} = -7,500$	[16]
$Al_{13}Fe_4$	$(Al,Zn)_{0.6275}(Fe)_{0.235}(Al,Va)_{0.1375}$	Fe–Al	$\Delta G^{f}_{Fe-Al} = -30,714.4 + 7.44 \times T$	[16]
		Fe–Al–Zn	$\Delta G^{f}_{Fe-Al-Zn} = -7,500$	[16]
		Al–Fe–Va	$\Delta G^{f}_{Fe-Al-Va} = -27781.3 + 7.2566 \times T$	[16]
Al_7Cr	$(Al)_{0.75}(Cr)_{0.1333}(Al,Zn)_{0.1167}$	Cr–Al	$\Delta G^{f}_{Cr-Al} = -13,389 + 0.479 \times T$	[26]
		Cr–Al–Zn	$\Delta G^{f}_{Cr-Al-Zn} = -15,000$	[13]
Al_2Cr_3	$(Al)_{0.4}(Cr)_{0.5}(Cr,Zn)_{0.1}$	Cr–Al	$\Delta G^{f}_{Cr-Al} = -19,500$	[26]
		Cr–Al–Zn	$\Delta G^{f}_{Cr-Al-Zn} = -18,000$	[13]
Al_4Cr	$(Al)_{0.8}(Cr)_{0.2}$	Cr–Al	$\Delta G^{f}_{Cr-Al} = -17,154 + 0.25 \times T$	[26]
Al_8Cr_5	$(Al)_{0.6}(Cr)_{0.4}$	Cr–Al	$\Delta G^{f}_{Cr-Al} = -15,062 - 8.496 \times T$	[26]
Al_9Cr_4	$(Al)_{0.692}(Cr)_{0.308}$	Cr–Al	$\Delta G^{f}_{Cr-Al} = -12,907 - 7 \times T$	[26]
$AlCr_2$	$(Al)_{0.333}(Cr)_{0.667}$	Cr–Al	$\Delta G^{f}_{Cr-Al} = -10,878 - 8.299 \times T$	[26]
τ_4	$(Al,Zn)_{0.48}(Cr)_{0.1207}(Zn)_{0.3993}$	Al–Cr–Zn	$\Delta G^{f}_{Al-Cr-Zn} = -300$	[13]
		Cr–Zn	$\Delta G^{f}_{Cr-Zn} = -400$	[13]

parameters are given in the appendix together with the parameters selected from literature.

Thermodynamic models

Unary phases

The Gibbs energy function ${}^{\circ}G_i^{\varphi}(T) = G_i^{\varphi}(T) - H_i^{\mathrm{SER}}$ for the element i (i = Fe, Cr, Zn, Al) in the phase φ [φ = liquid, body-centered cubic (bcc), hexagonal close-packed (hcp), face-centered cubic (fcc)] is given by the following expression:

$$ {}^{\circ}G_i^{\varphi}(T) = a + bT + cT\ln T + dT^2 + eT^3 + fT^{-1} + hT^{-9} \quad (1) $$

where H_i^{SER} is the molar enthalpy of the element i at 298.15 K in its standard element reference (SER) state, bcc for Fe and Cr, fcc for Al and hcp for Zn. The Gibbs energy of the element i in its SER state is denoted by GHSERi, i.e.:

$$\mathrm{GHSERFE} = G_{\mathrm{Fe}}^{\mathrm{bcc}}(T) - H_{\mathrm{Fe}}^{\mathrm{SER}} \quad (2)$$

$$\mathrm{GHSERCR} = G_{\mathrm{Cr}}^{\mathrm{bcc}}(T) - H_{\mathrm{Cr}}^{\mathrm{SER}} \quad (3)$$

$$\mathrm{GHSERZN} = G_{\mathrm{Zn}}^{\mathrm{hcp}}(T) - H_{\mathrm{Zn}}^{\mathrm{SER}} \quad (4)$$

$$\mathrm{GHSERAL} = G_{\mathrm{Al}}^{\mathrm{fcc}}(T) - H_{\mathrm{Al}}^{\mathrm{SER}} \quad (5)$$

In the present work, Gibbs energy functions of pure elements are taken from the SGTE compilation [19].

Solid and liquid solutions

In the Fe–Cr–Zn–Al system, no quaternary interaction parameters were used. The Gibbs energy of the ternary solution phases is described by the following expressions (i, j, and k represent 3 elements among Fe, Cr, Al, and Zn):

$${}^{\circ}G_{\mathrm{m}}^{\varphi}(T) = G_{\mathrm{m}}^{\varphi}(T) - x_i H_i^{\mathrm{SER}} - x_j H_j^{\mathrm{SER}} - x_k H_k^{\mathrm{SER}} \quad (6)$$

$$\begin{aligned}{}^{\circ}G_{\mathrm{m}}^{\varphi}(T) = {} & x_i {}^{\circ}G_i^{\varphi} + x_j {}^{\circ}G_j^{\varphi} + x_k {}^{\circ}G_k^{\varphi} \\ & + RT\left(x_i \ln x_i + x_j \ln x_j + x_k \ln x_k\right) + {}^{\mathrm{xs}}G_{\mathrm{m}}^{\varphi}(T)\end{aligned} \quad (7)$$

where ${}^{\mathrm{xs}}G_{\mathrm{m}}^{\varphi}$ is the excess Gibbs energy, expressed by a Redlich–Kister polynomial:

$$\begin{aligned}{}^{\mathrm{xs}}G_{\mathrm{m}}^{\varphi}(T) = {} & x_i x_j \sum_{v=0}^{n} L_{i,j}^{v}(x_i - x_j)^v + x_j x_k \sum_{v=0}^{n} L_{j,k}^{v}(x_j - x_k)^v \\ & + x_k x_i \sum_{v=0}^{n} L_{k,i}^{v}(x_i - x_k)^v + L_{ijk} x_i x_j x_k\end{aligned} \quad (8)$$

where $L_{i,j}^{v}$ is the interaction parameter between elements i and j in the phase φ. It is generally a linear function of temperature:

$$L_{i,j}^{v} = a_{i,j}^{v} + b_{i,j}^{v} T \quad (9)$$

and L_{ijk} is a ternary interaction parameter between 3 elements among Fe, Cr, Al, and Zn.

Stoichiometric compounds

The Gibbs energy per mole formula unit $i_{\mathrm{m}}j_{\mathrm{p}}$ is expressed as follows:

$${}^{\circ}G_{\mathrm{m}}^{i_{\mathrm{m}}i_{\mathrm{p}}}(T) = G_{\mathrm{m}}^{i_{\mathrm{m}}j_{\mathrm{p}}}(T) - \mathrm{m}H_i^{\mathrm{SER}} - \mathrm{p}H_j^{\mathrm{SER}} \quad (10)$$

$${}^{\circ}G_{\mathrm{m}}^{i_{\mathrm{m}}j_{\mathrm{p}}}(T) = \mathrm{mGHSER}i + \mathrm{pGHSER}j + \Delta_f G^{i_{\mathrm{m}}j_{\mathrm{p}}} \quad (11)$$

where $\Delta_f G^{i_{\mathrm{m}}j_{\mathrm{p}}}$ is the Gibbs energy of formation per mole of formula unit $i_{\mathrm{m}}j_{\mathrm{p}}$:

$$\Delta_f G^{i_{\mathrm{m}}j_{\mathrm{p}}} = \Delta_f H^{i_{\mathrm{m}}j_{\mathrm{p}}} - T\Delta_f S^{i_{\mathrm{m}}j_{\mathrm{p}}} \quad (12)$$

Due to a lack of experimental measurements, it is assumed that Neumann–Kopp's rule is applied to the heat capacity of the compounds. Hence $\Delta_f H^{i_{\mathrm{m}}j_{\mathrm{p}}}$ and $\Delta_f S^{i_{\mathrm{m}}j_{\mathrm{p}}}$ are considered as independent of temperature.

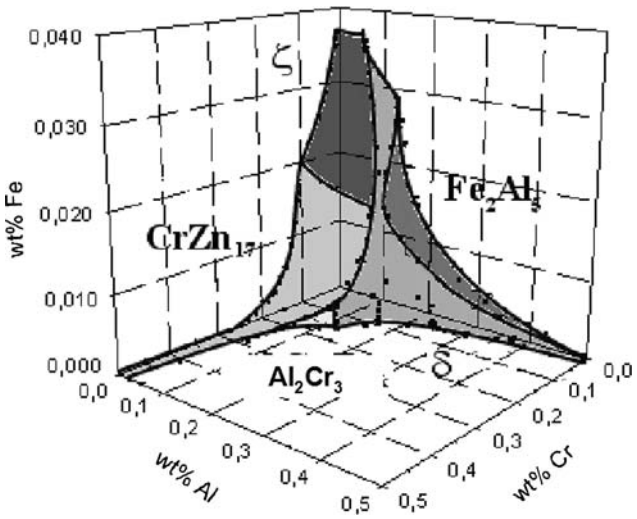

Fig. 5 Optimized liquidus in the Fe–Zn–Al–Cr system at 460 °C. Black spots represent experimental borders between $CrZn_{17}$ and $\delta(\tau_1)$ and between the phases in the ternary systems

Assessment procedure

The solid phases stable at 460 °C are presented in Table 2. Optimization, by the Parrot module, of the quaternary liquidus at 460 °C, was achieved from 3 optimized ternary systems: Fe–Zn–Al [6], Fe–Zn–Cr [3], and Al–Cr–Zn [4]. In order to simplify calculations, the solid phases were described as stoichiometric by using a system of substitution in sublattices. Expressions of the assessed thermochemical parameters are presented in Tables 3 and 4.

This optimized isothermal liquidus of the Fe–Zn–Al–Cr at 460 °C is shown in Fig. 5. Owing to the identification $\delta = \tau_1$, the liquid phase is in equilibrium with 5 solid phases namely δ, Fe_2Al_5, Al_2Cr_3, $CrZn_{17}$, and ζ. These phases, with the exception of δ, are nearly stoichiometric. Fe_2Al_5 is actually saturated with Zn [$Fe_2(Al_{1-x}Zn_x)_5$ with $x \sim 0.15$]; Al_2Cr_3, metastable, is stabilized by Zn ($Al_2Cr_3Zn_x$ with $x \sim 0$); $CrZn_{17}$ is saturated with Fe [$Cr(Fe_xZn_{1-x})_{17}$ with $x \sim 0.01$]. Only a small part of the liquidus surface is in equilibrium with Fe_2Al_5.

Discussion

The optimization of the Fe–Zn–Al–Cr system at 460 °C by Thermo-Calc allowed us to understand the solid/liquid phase equilibria and the formation of the precipitates and intermetallic layers when iron substrates were dipped in a molten zinc bath. To explain the formation of Fe_2Al_5 in δ dross observed in Fig. 4, different sequences of gradual

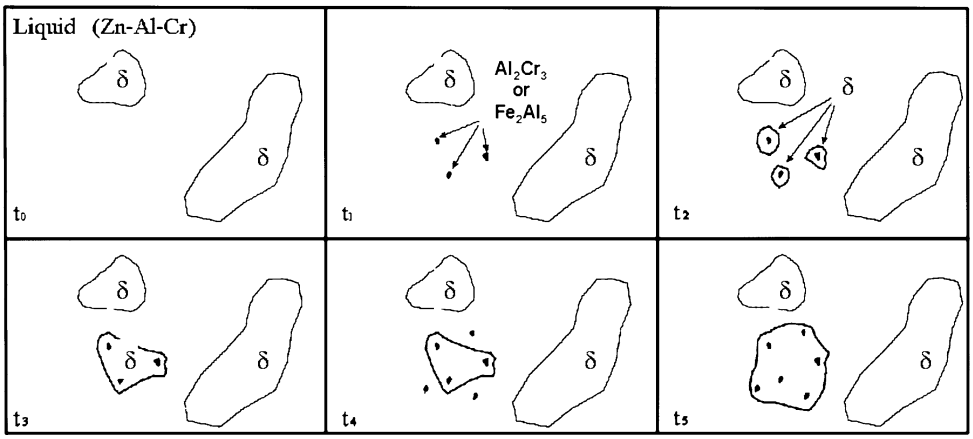

Fig. 6 Modeling the growth of the dross formation when iron is added in an Al–Cr–Zn bath at 460 °C

additions of Fe in Al–Cr–Zn bath at 460 °C were presented in a model (Fig. 6). Time $t = 0$ corresponds to the beginning of the experiment when iron was added to the bath, and t_5 corresponds to a long period after the last iron addition.

At time $t = 0$, in the system Al–Cr–Zn at 460 °C, the liquid phase is thermodynamically in equilibrium with the solid phase δ. Industrial zinc bath enriched with Al is initially saturated with iron. At time t_1, when steel strip is dipped in the bath, experiment shows that zinc bath over saturates with Fe before any precipitation of intermetallic compounds. Fe in excess, instead of precipitating to form Fe–Zn intermetallic compounds (δ or ζ), precipitates as $Fe_2(Al_{1-x}Zn_x)_5$ intermetallic compound because of the strong affinity between iron and aluminum. $Fe_2(Al_{1-x}Zn_x)_5$ is present both in the dross of the bath and at the surface of steel strip. The $Fe_2(Al_{1-x}Zn_x)_5$ layer coating the steel strip is usually known as inhibition layer because it prevents the formation of Fe–Zn intermetallic compounds on the steel strip. Actually experimental diffusion path in quaternary diagram is liquid Zn–$Fe_2(Al_{1-x}Zn_x)_5$–Fe. However, according to the diagram Fe–Zn–Al–Cr at 460 °C, these $Fe_2(Al_{1-x}Zn_x)_5$ precipitates are not in thermodynamic equilibrium with the liquid zinc bath. Thus, at time t_2, the solid phase δ precipitates around the first $Fe_2(Al_{1-x}Zn_x)_5$ dross, until the thermodynamic equilibrium at the solid–liquid interface be reached. This solidification of the δ phase is followed, at time t_3, by growth and coalescence of the dross. As a consequence, the precipitation and growth involve local zinc depletion together with enrichment in aluminum, chromium, and iron. At time t_4, new $Fe_2(Al_{1-x}Zn_x)_5$ dross form in the vicinity of the δ dross containing the first $Fe_2(Al_{1-x}Zn_x)_5$ intermetallic compounds. Finally, at time t_5, according to thermodynamic equilibrium between the liquid and the δ phase, the δ dross grows until the disappearance of the last $Fe_2(Al_{1-x}Zn_x)_5$ crystals formed in the vicinity.

The thermodynamic optimization of quaternary system at 460 °C can also explain the presence of δ compounds in the inhibition layer $Fe_2(Al_{1-x}Zn_x)_5$ during galvanizing. A microscopic observation of the inhibition layer coming from the 0.200 mass% Al–0.050 mass% C–0.012 mass% Fe bath shows two main zones. A brighter zone is the matrix identified as $Fe_2(Al_{1-x}Zn_x)_5$; darker polyhedral precipitates were analyzed as δ. The δ presence inside the $Fe_2(Al_{1-x}Zn_x)_5$ layer confirms our results about the liquidus of the Fe–Zn–Al–Cr. Indeed, the chromium solubility in the liquid was evaluated at 0.040 mass%: an equilibrium between 3 phases liquid + δ + $Fe_2(Al_{1-x}Zn_x)_5$ is observed.

Conclusions

The optimization of the Fe–Zn–Al–Cr system at 460 °C gives boundary limits which are consistent with the experimental diagram and is a basis for the explanation of the formation and growth of precipitates or layer during galvanizing. The Cr added in the bath favored the formation of δ phase at the expense of $Fe_2(Al_{1-x}Zn_x)_5$. The chromium solubility in the liquid decreases when the Al content of the bath increases. On another hand, the liquidus surface in equilibrium with $Fe_2(Al_{1-x}Zn_x)_5$ shrinks when the Cr content of the liquid increases. Above 0.1 mass% Cr in the liquid, the precipitation of $Fe_2(Al_{1-x}Zn_x)_5$ dross is no more possible. This result suggests that the presence of Cr in the liquid avoids the formation of an inhibition layer.

Acknowledgement The authors would like to thank UMICORE Research and the ARCELOR Research Centre (OCAS) for their financial support and their interest in the development of this technical innovation.

References

1. Tang NY, Adams GR (1993) In: Marder AR (ed) Phys. metallurgy of zinc coated steel. TMS, Materials Park, OH, p 41
2. Perrot P, Tissier JC, Dauphin JY (1992) Z Metallkd 83:785
3. Tang NY (2000) J Phase Equilib 21(1):70

4. McDermitt JR, Kaye MH, Thompson WT (2007) Metall Mater Trans B 38B(2):215. doi:10.1007/s11663-007-9028-3
5. Gyurov S (1997) Z Metallkd 88(4):346
6. Tang NY, Yu XB, Coady FN (2003) Metall Mater Trans A 34A(3a):879
7. Nakano J, Malakhov DV, Yamaguchi S, Purdy GR (2007) Calphad 31(1):125. doi:10.1016/j.calphad.2006.09.003
8. Giorgi ML, Guillot JB, Nicolle R (2001) Calphad 25(3):461. doi:10.1016/S0364-5916(01)00065-7
9. Bai K, Wu P (2002) J Alloy Compds 347:156
10. Reumont G, Mathon M, Fourmentin R, Perrot P (2003) Z Metallkd 94:411
11. Tang NY, Yu XB (2005) J Phase Equilib Diff 26(1):50
12. Raghavan V (2007) J Phase Equilib Diff 28(4):383
13. Fourmentin R, Avettand-Fenoel MN, Reumont G, Perrot P (2007) J Mater Sci 42:7934. doi:10.1007/s10853-007-1521-1
14. Watanabe H, Sato E (1969) Keikinzoku 19(11):499
15. Reumont G, Perrot P (2003) J Phase Equilib 24:50
16. David N (2001) Thesis, University Henri Poincaré, Nancy
17. Reumont G (1990) Thesis, Université des Sciences et Technologies de Lille
18. Sundman B, Jansson B, Anderson JO (1985) Calphad 9:153. doi:10.1016/0364-5916(85)90021-5
19. Dinsdale AT (1991) Calphad 15:317. doi:10.1016/0364-5916(91)90030-N
20. Massalski TB (1990) Binary alloy phase diagram, 2nd edn. ASM, Materials Park, OH
21. Raghavan V (1992) Phase diagrams of ternary iron alloys, vol 6A. Indian Inst. Metals, Calcutta
22. Moser Z, Heldt LA (1992) J Phase Equilib 13(2):172
23. Grushko B, Przepiorzynski B, Pavlyuchkov D (2008) J Alloy Compds 454:214
24. Villars P, Calvert LD (1991) Pearson's handbook of crystallographic data for intermetallic phases, 2nd edn. ASM, Materials Park, OH
25. Grushko B, Kowalska-Strzeciwilk E, Przepiorzynski B, Surowiec M (2005) J Alloy Compds 402:98
26. Saunders N, Rivlin VG (1987) Z Metallkd 78:795